Impact of Marginal Exciton-Charge-Transfer State Offset on Charge Generation and Recombination in Polymer

Vezie, Michelle S.; Azzouzi, Mohammed; Telford, Andrew M.; Hopper, Thomas R.; Sieval, Alexander B.; Hummelen, Jan C.; Fallon, Kealan; Bronstein, Hugo; Kirchartz, Thomas; Bakulin, Artem A.

Published in:
ACS Energy Letters

DOI:
10.1021/acsenergylett.9b01368

Publication date:
2019

ACS Energy LETTERS

Cite This: ACS Energy Lett. 2019, 4, 2096−2103

http://pubs.acs.org/journal/aelccp

LETTER

Impact of Marginal Exciton−Charge-Transfer State Offset on Charge Generation and Recombination in Polymer:Fullerene Solar Cells

Michelle S. Vezie,[†,¶] Mohammed Azzouzi,[†,¶] Andrew M. Telford,[†] Thomas R. Hopper,[‡] Alexander B. Sieval,[§] Jan C. Hummelen,[§,∥] Kealan Fallon,[⊥] Hugo Bronstein,[#] Thomas Kirchartz,[∇,○] Artem A. Bakulin,[‡] Tracey M. Clarke,[⊥] and Jenny Nelson*[,†]

[†]Department of Physics and Centre for Plastic Electronics, Imperial College London, London SW7 2AZ, United Kingdom

[‡]Department of Chemistry and Centre for Plastic Electronics, Imperial College London, London SW7 2AZ, United Kingdom

[§]Solenne BV, Zernikepark 6, 9747AN Groningen, The Netherlands

[∥]Stratingh Institute for Chemistry & Zernike Institute for Advanced Materials, University of Groningen, Nijenborgh 4, 9747AN Groningen, The Netherlands

[⊥]Department of Chemistry, University College London, Christopher Ingold Building, London WC1H 0AJ, United Kingdom

[#]Department of Chemistry, University of Cambridge, Lensfield Road, Cambridge, CB2 1EW, United Kingdom

[∇]IEK5-Photovoltaics, Forschungszentrum Jülich, 52425 Jülich, Germany

[○]Faculty of Engineering and CENIDE, University of Duisburg−Essen, Carl-Benz-Strasse 199, 47057 Duisburg, Germany

Supporting Information

ABSTRACT: The energetic offset between the initial photoexcited state and charge-transfer (CT) state in organic heterojunction solar cells influences both charge generation and open-circuit voltage (V_{oc}). Here, we use time-resolved spectroscopy and voltage loss measurements to analyze the effect of the exciton−CT state offset on charge transfer, separation, and recombination processes in blends of a low-band-gap polymer (INDT-S) with fullerene derivatives of different electron affinity (PCBM and KL). For the lower exciton−CT state offset blend (INDT-S:PCBM), both photocurrent generation and nonradiative voltage losses are lower. The INDT-S:PCBM blend shows different excited-state dynamics depending on whether the donor or acceptor is photoexcited. Surprisingly, the charge recombination dynamics in INDT-S:PCBM are distinctly faster than those in INDT-S:KL upon excitation of the donor. We reconcile these observations using a kinetic model and by considering hybridization between the lowest excitonic and CT states. The modeling results show that this hybridization can significantly reduce V_{oc} losses while still allowing reasonable charge generation efficiency.

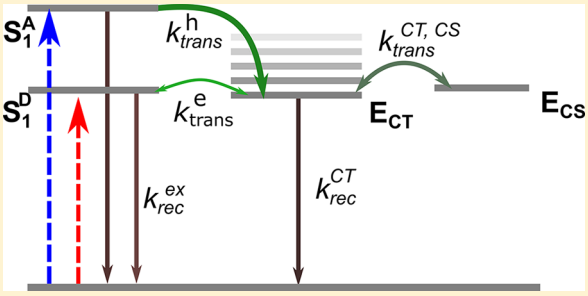

In organic solar cells, the heterojunction between electron donor and electron acceptor materials provides the driving energy for charge separation, as well as the interface at which recombination occurs.[1] In the common picture of device function, both charge separation and charge recombination proceed via a manifold of excitonic and charge-transfer (CT) excited states that extend locally over donor and/or acceptor media.[2−6] The driving energy can be quantified as the energetic offset between the local photoexcited exciton (localized on the donor or the acceptor) and the lowest-energy CT state (localized across the interface with positive charge on the donor and negative charge on the acceptor). While some reports have indicated that charge generation efficiency decreases when this offset is reduced,[7−9] others have reported efficient pair generation at apparently negligible offsets in polymer:fullerene[10] and, increasingly, in polymer:nonfullerene acceptor[11] blends. Consequently, the effect of the

Received: June 26, 2019
Accepted: August 6, 2019
Published: August 6, 2019

DOI: 10.1021/acsenergylett.9b01368
ACS Energy Lett. 2019, 4, 2096−2103

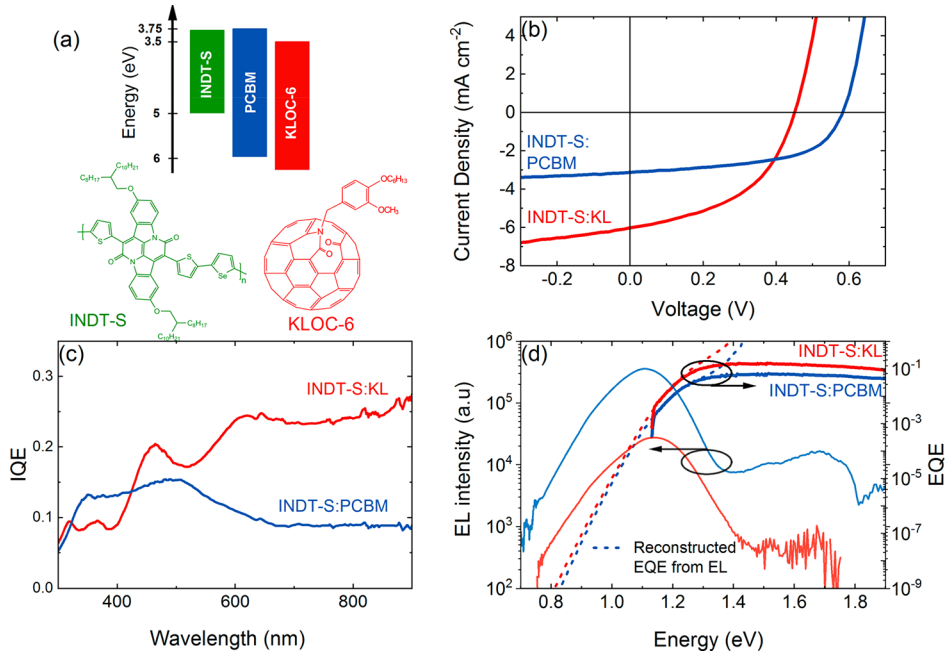

Figure 1. (a) Chemical structures of INDT-S and KLOC-6 (KL in this paper), with the HOMO and LUMO levels as calculated using CV and photoelectron spectroscopy. (b) *J*–*V* characteristics of the two blends INDT-S:PCBM and INDT-S:KL and (c) IQE of the two devices as calculated using the method presented in the SI. (d) EQE and EL of the two devices, with the extended EQE using the reciprocity between EL and EQE. The EL spectra are taken for an injection current of 20 mA cm^{-2}.

driving force and the excitation energy on charge pair generation remains controversial.[12−14]

While a large offset may benefit photocurrent, smaller offsets benefit the open-circuit voltage (V_{oc}). Organic solar cells tend to show smaller qV_{oc} (where q is electronic charge) relative to the optical gap than good inorganic solar cells.[15] qV_{oc} is empirically linked to the energy of the lowest CT state, E_{CT}.[16] The relatively low V_{oc} can be assigned partly to the presence of the heterojunction, which limits the energy gap between electron and hole quasi-Fermi levels relative to the gap achievable in either the donor or acceptor material alone, and partly to the relatively high rate of nonradiative recombination that is observed in organic heterojunction solar cells.[17,18] The second component, the loss in V_{oc} due to nonradiative recombination, can be quantified as $\Delta V_{oc,nr} = \frac{kT}{q}\ln\left(\frac{1}{QE_{EL}}\right)$, where QE_{EL} is the radiative quantum efficiency of the device. While the best silicon solar cell has $\Delta V_{oc,nr} < 0.11$ V (QE_{EL} >1%),[19] organic donor:acceptor heterojunction solar cells have $\Delta V_{oc,nr}$ in the range of 0.20−0.55 V, with QE_{EL} usually well below 10^{-3}%.[11,15,20,21]

In an attempt to increase solar cell performance, V_{oc} could be raised by reducing the energetic offset. However, this would also reduce the driving force for charge separation and may compromise the charge separation efficiency or enhance geminate recombination. A relevant question, therefore, is how far can the V_{oc} be raised by reducing the energetic offset at the heterojunction without deteriorating the device performance: *in particular, how does a small offset influence recombination kinetics?* A further question in understanding the mechanism of interfacial CT processes is how the choice of photoexcited component (donor or acceptor) influences the CT efficiency and recombination kinetics, given that the donor and acceptor excitons, in general, present different offsets relative to the CT state.

In this work, we study a low-band-gap polymer combined with two different fullerene derivatives, which both possess large offsets for hole transfer but different offsets for electron transfer. We use ultrafast transient absorption and pump−push-photocurrent spectroscopy to show that, upon excitation of the donor, the lower-offset blend exhibits shorter charge lifetimes, despite higher V_{oc} and a lower $\Delta V_{oc,nr}$. By modeling the nonradiative recombination via the CT state and a kinetic model, we can explain this behavior in terms of the impact of CT and singlet state mixing on the oscillator strength of the CT state. The results suggest a useful design rule for high-voltage organic solar cell materials.

Material System and Device Performance. We study the low-band-gap isoindigoid-based polymer indolo-naphthyridine-6,13-dione thiophene-*co*-selenophene (INDT-S)[22] combined with two [60]fullerene derivatives of different electron affinity: the widely studied phenyl C_{61} butyric acid methyl ester (PCBM) and a new ketolactam fullerene derivative KLOC-6 (KL) (see section S1 for synthesis details). The molecular structures and energies of the highest occupied molecular orbital (HOMO) and lowest unoccupied molecular orbital (LUMO) of these molecules are shown in Figure 1a. The INDT-S:PCBM system presents a nominal LUMO(Donor) − LUMO(Acceptor) difference of −0.02 eV, taking the INDT-S LUMO as −3.77 eV (from a photoelectron spectroscopy estimate of the HOMO energy plus the optical gap[23]) and the PCBM LUMO as −3.75 eV [from cyclic voltammetry (Table S1 and Figure S1)]. The LUMO of KLOC-6 lies 170 meV deeper than PCBM, also determined by CV, leading to a LUMO difference of around 0.15 eV for the INDT-S:KL blend. The HOMO energy differences are large (>0.5 eV) in both blends. Although the estimates of the offset energies in blend films are uncertain[22] (due to differences in the measurement technique to estimate HOMO and LUMO energies and uncertainties in translating MO energy differences

DOI: 10.1021/acsenergylett.9b01368
ACS Energy Lett. 2019, 4, 2096−2103

Table 1. Solar Cell Parameters Extracted from the $J-V$ Curves and from the Luminescence-Based Voltage Loss Analysis for the Two Blends[a]

blend	J_{sc} [mA/cm^2]	PCE [%]	FF	V_{oc} [V]	$V_{oc,rad}$ [V]	$\Delta V_{oc,nr}$[V]
INDT-S:KL	6.02	1.28	0.46	0.46	0.94	0.48
INDT-S:PCBM	3.12	1.01	0.56	0.58	0.93	0.35

[a]PCE is the power conversion of the cell under AM1.5G equivalent light intensity, and FF is the fill factor.

into state energy offsets), the two combinations represent a medium-offset and low-offset donor:acceptor blend for electron transfer. Because both fullerenes are C_{60} derivatives, their optical absorption properties are almost identical, leading to very similar absorption profiles for the blend films (Figure S2). For both blends, the donor absorption (maximum at 600−900 nm) is spectrally separated from the acceptor absorption (<500 nm). This spectral separation allows the donor and acceptor components to be selectively excited, thereby triggering electron-transfer and hole-transfer pathways, respectively.

Current density−voltage ($J-V$) and internal quantum efficiency (IQE, defined as the current collected per photon absorbed) data are displayed in Figure 1b,c. Sample and device preparation details are given in the Experimental Methods section of the SI. The data clearly show that more current is generated, per absorbed photon, from excitation of the polymer in the KL blend than that in the PCBM blend, resulting in greater overall short-circuit current density (J_{sc}). Furthermore, there is no evidence of wavelength-dependent photogeneration efficiency within the region where only the polymer absorbs, in contrast to some previous reports.[4] At shorter wavelengths, the data are more susceptible to interference effects.[24] Therefore, a reliable comparison of the two spectra in the region where the acceptor absorbs (<500 nm) cannot be made. The IQE was calculated using the external quantum efficiency (EQE) in conjunction with experimental reflectivity measurements and the parasitic absorption. The latter was simulated from the experimental complex refractive index data and an optical model;[25] see section S3 for full details. Although the efficiency of current generation from the polymer is higher in the high-offset KL blend, it is clearly not negligible in the low-offset PCBM blend. For comparison, the EQE of a pristine INDT-S device is no greater than 0.05%, suggesting an IQE of ≪0.5% (Figure S4).

Figure 1c shows that the V_{oc} of the KL blend under AM1.5 illumination is smaller than that of the PCBM blend, as would be expected from the smaller LUMO offset. To quantify the voltage difference, we measure the electroluminescence (EL) and high-dynamic-range EQE spectra of both blends (Figures 1d and 5a) to extract the V_{oc} in the radiative limit, $V_{oc,rad}$, and the nonradiative voltage loss $\Delta V_{oc,nr} = V_{oc,rad} - V_{oc}$ (Table 1; see ref 15 for details of the method and Figure S5b for the full data). The calculated $V_{oc,rad}$ is almost identical for the two blends despite the significant difference in energy level offsets. Meanwhile, $\Delta V_{oc,nr}$ for the INDT-S:KL device (0.48 V) is 0.1 V larger than that for the INDT-S:PCBM device (0.35 V). Correspondingly, the QE_{EL} is larger in the PCBM device, resulting in a greater EL intensity than that of the KL device under a similar injection current.

Spectroscopy Measurements. To better understand the kinetics of the excited species, we study films of both blends using transient absorption spectroscopy (TAS). μs-TAS yields the spectra of long-lived species in the blends, in all cases consisting of a broad feature centered at around 1600 nm, assigned to the excited states of the polymer, which may include positive polarons and triplets, and a band at 1100−1300 nm assigned to the fullerene anion (Figure S6). By comparing the amplitude of the polymer excited-state absorption at late times (400 ns) after 709 nm excitation (Figure S6), it is clear that long-lived excited-state generation following selective polymer excitation is approximately twice as efficient in the high-offset KL blend as in the low-offset PCBM blend. This observation is consistent with the excited-state signal being primarily due to positive polymer polarons. For both blends, the TA spectra are identical in shape regardless of polymer or fullerene excitation, suggesting that the same long-lived species are generated on the μs time scale irrespective of which component is initially photoexcited. The low band gap of the polymer suggests that its triplet states would have an even lower energy; therefore, we cannot rule out their presence even though the TA dynamics appear to be insensitive to oxygen (Figure S7). The role of triplets in the ps-TAS dynamics may safely be neglected given that the time scale for intersystem crossing is usually longer than the characteristic times for dissociation of the photoexcited state.[26]

To examine the shorter-lived states, we performed ps-TAS on both blend films following excitation of the polymer alone (800 nm pump) or predominant excitation of the fullerene derivative (450 nm pump). The TA spectra for all of the blends contain a broad feature, peaking above 1300 nm, which is assigned to the photoinduced absorption by the INDT-S exciton (Figure S8). On the ns time scale, the spectra of both blends show features in the 1000−1300 nm region, which resemble the fullerene anion signature observed in the μs-TAS data.[27] The interconversion dynamics of these species can be probed at 1200 nm, where the photoinduced absorption signals from the charged species and polymer singlet exciton overlap (Table S2).

Figure 2 shows the ps-TAS kinetics of the blends probed at 1200 nm after donor or acceptor excitation. When pumped at 800 nm (Figure 2a), the INDT-S:PCBM blend shows a fast, approximately exponential, decay with a ∼20 ps lifetime, while the INDT-S:KL blend decays much more slowly, with almost 25% of the initial signal amplitude still present after 6 ns. Somewhat surprisingly, the ps-TAS kinetics of the pristine polymer and INDT-S:PCBM blend are almost identical following 800 nm excitation. Both materials show exponential kinetics with a ∼20 ps lifetime, consistent with a previous report for the polymer S_1 state lifetime (23 ps).[23] This is unexpected as the TA spectra (Figure S8) and device characteristics for INDT-S:PCBM (Table 1) clearly show evidence of charge generation. Assuming that the assignment of the 1050−1250 nm feature to fullerene anions is correct, the kinetics would suggest that INDT-S:PCBM undergoes both ultrafast charge generation and very rapid geminate recombination. The short lifetime of these states is consistent with the notion of tightly bound charge pairs in this low-offset system.[28]

In contrast, pumping the blends at 450 nm leads to slow, multiphasic TAS decays for both blends (Figure 2b), similar in

DOI: 10.1021/acsenergylett.9b01368
ACS Energy Lett. 2019, 4, 2096−2103

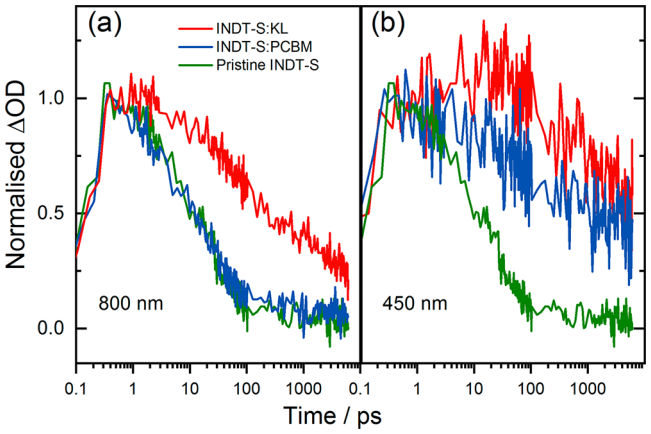

Figure 2. ps-TAS kinetics of INDT-S:PCBM and INDT-S:KL blend films probed at 1200 nm after excitation at 800 (a) and 450 nm (b) under similar excitation fluences (9 and 14 μJ cm^{-2}, respectively). For comparison, the kinetics for the pristine INDT-S film (obtained with 800 nm excitation, 9 μJ cm^{-2}) are shown in both cases.

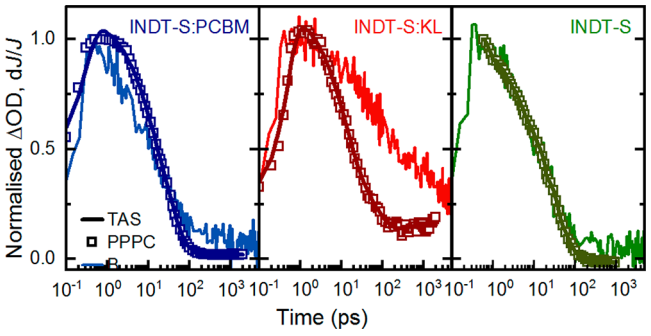

Figure 3. Kinetics of the ps-TAS of INDT-S:PCBM and INDT-S:KL blend films and pristine INDT-S probed at 1200 nm, compared to the normalized PPPC signal with an excitation at 800 nm and a push wavelength of 2000 nm.

kinetics to the KL blend when pumped at 800 nm, and with evidence for fullerene anion generation (Figure S8). At this 450 nm pump wavelength, primarily the fullerene is excited; therefore, hole (rather than electron) transfer should follow. We assume that energy transfer from the fullerene to the polymer is negligible compared to the efficiency of CT, given that both blends have a high offset for hole transfer. The ps-TAS data thus provide evidence for long-lived charges in all cases where there is a high exciton−CT state offset to drive charge separation and, conversely, rapid decay of charges where a low offset is concerned.

In order to probe the nature of the photoexcited species in the blends at ps time scales, we performed visible pump−IR push-photocurrent detection (PPPC).[6,29] A 2000 nm wavelength push laser was used to excite the bound photoexcited states to higher-energy, more delocalized states without further excitation of the ground state. Devices were measured under identical conditions with the push-induced photocurrent (dJ) normalized to the reference photocurrent (J). Therefore, the absolute values of dJ/J can be directly compared and should reflect the relative fraction of bound charge pairs in these systems. For both blends, the yield of initial bound charges is greater under 800 nm excitation, where only electron transfer is possible (Figure S9a). Here, dJ/J from the PCBM blend is 1 order of magnitude larger than that in the KL blend, indicating a larger initial population of bound charges. This points to a lower efficiency for charge separation, which is consistent with the overall device performance and can be explained by a reduced driving force for charge separation. At 400 nm excitation, where hole transfer dominates the photophysics of both materials and the charge separation driving force is greater, we observe a much lower number of initial bound charge pairs for both blends. Comparatively, the KL blend still exhibits fewer bound charges than the PCBM blend.

The kinetics from the PPPC and ps-TAS data following 800 nm excitation for the two blends, as well as the pristine INDT-S, are directly compared in Figure 3. It is clear from these data that the decay of the PPPC and ps-TAS signals following polymer excitation are very similar for the INDT-S:PCBM case. However, for the INDT-S:KL case, the kinetics from the two experiments are very different. TAS gives a measure of all charges, while PPPC is sensitive to only bound charges. Therefore, this comparison clearly shows that for 800 nm excitation in the INDT-S:KL blend significant numbers of unbound (free) charges are being generated, which exhibit a longer lifetime than the bound charges that are monitored by PPPC. Meanwhile, for 800 nm excitation in the PCBM blend and in the pure polymer, the decay is dominated by bound charge pairs that are generated quickly (<1 ps) but recombine rapidly in the absence of the push pulse. For the 400 nm excitation, the decay of the photoexcited charges for the two blends probed using TAS and the PPPC experiment are similar to the case of the INDT-S:KL blend probed at 800 nm, i.e., showing a slow shoulder in the TAS signal, confirming the generation of a significant number of unbound charges (Figure S9b). This points toward the push-induced separation of excitons, which has been previously observed in pristine polymer devices.[30]

Time-Dependent Density Functional Calculations of the Excited States. To characterize the interfacial states further, we calculated the excited states for the donor (modeled as a dimer of INDT-S), the fullerene acceptor, and the donor:-acceptor pair for each fullerene type using density functional theory (DFT) (B3LYP/6-31G*) and time-dependent DFT (TDDFT); see SI section S11 for details.[31] Although a two-molecule system is a crude model for an organic blend film that supports many more excited states[32,33] and CT character may not be well modeled by TDDFT, these calculations serve as a guide to the nature of the lowest excited states. Calculations for the individual donor and acceptor support the smaller LUMO−LUMO energy difference for INDT-S:PCBM than INDT-S:KL that is expected from experimental data. In comparing the two donor:acceptor pairs, the first singlet excited states lie at similar energies, but the INDT-S:KL state has much stronger CT character (0.8 as opposed to 0.1 for the INDT-S:PCBM, charge transferred from the donor to the acceptor) and an order-of-magnitude lower oscillator strength (f_{OSC}) for the transition to the ground state compared to that for INDT-S:PCBM. The mixed excitonic−CT nature of the lowest INDT-S:PCBM state suggests hybridization of the donor exciton and the CT state, consistent with the intensity-borrowing effect.[34] This hybridization effect and associated effect on oscillator strength can also be inferred from the EL data. The similar positions of the EL peaks for pristine and blend films suggest that the polymer and CT state emission are mixed, with much brighter EL from the PCBM than KL blends (see Figure S5a), in accordance with the trend in f_{OSC}.

DOI: 10.1021/acsenergylett.9b01368
ACS Energy Lett. 2019, 4, 2096−2103

We now endeavor to explain the different charge generation and recombination behavior of the two blend systems. To summarize the observations, both blend devices showed efficient charge generation as compared to the pristine donor device, regardless of which component (donor or acceptor) is excited, but charge generation following polymer excitation is twice as efficient for the KL than the PCBM blend. The evolution of the excited states as inferred from TAS and PPPC measurements appeared to be mostly affected by the difference in energy between the photogenerated exciton and the CT state: (1) when the difference is significant (exciting the acceptor in either case and exciting the donor in the KL case), photoexcited species decay slowly on a several ns time scale, and the slow kinetics are assigned to species that are unaffected by the IR perturbation in the PPPC experiment; (2) when the difference is small (exciting the donor in INDT-S:PCBM), the evolution of the excited states is similar to the pristine polymer case in both the TAS and the PPPC measurement; similar kinetics for TAS and PPPC suggest that the photogenerated charge pairs are bound. Moreover, the calculated excited states for blends using TDDFT suggest that the lowest excited state for the INDT-S:PCBM blend possesses more excitonic character (lower degree of charge transfer and higher f_{OSC}) than the INDT-S:KL case.

To explain the charge dynamics observed in the different cases, we propose the kinetic model in Figure 4a. In this

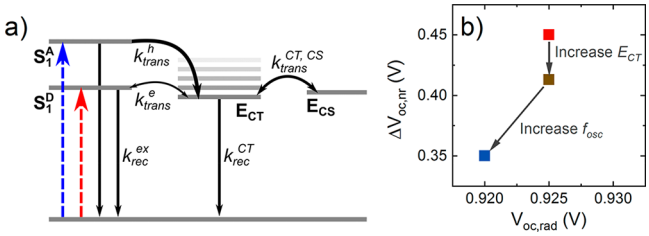

Figure 4. (a) State level diagram displaying the kinetic parameters in the model. (b) Model results for the nonradiative losses.

model, the initial exciton can (i) recombine with rate constant k_{rec}^{ex} or form a CT state via (ii) electron transfer, with rate constant k_{trans}^{e}, or (iii) hole transfer, with rate constant k_{trans}^{h}. The CT state can then either (iv) recombine with a rate constant k_{rec}^{CT} or (v) form a charge-separated (CS) state with a rate constant $k_{trans}^{CT,CS}$. The values of these rate constants, determined from the ps-TAS experiments, are detailed in Table 2, and supporting equations are given in section S12 of the SI.

The surprising similarity between the kinetics of pristine INDT-S and the INDT-S:PCBM blend after 800 nm excitation (Figure 2a) can be explained by slow electron transfer ($k_{trans}^{e} \approx 0.015$ ps^{-1}) in step (ii), which can be assigned to the low-energy difference between the lowest singlet donor exciton, S_1^D, and the CT state (E_{CT}). On the other hand, a faster hole transfer in the same blend, with rate constant $k_{trans}^{h} \approx 0.3$ ps^{-1}, reproduces the slower decay of the excited states when exciting the acceptor (450 nm) rather than the donor (Figure S12a). This difference in the net rates is expected given the larger energy of the lowest singlet acceptor exciton, S_1^D, because the large energy offset would increase the net rate of CT.[35] This reinforces the hypothesis that the difference in the charge generation process when the donor or acceptor is photoexcited can be explained by a difference in the rate of CT state

Table 2. Rate Parameters Used to Fit the ps-TA Spectra with the Kinetic Model[a]

	value (s^{-1})	
rate constant	INDT-S:PCBM	INDT-S:KL
k_{trans}^{e}	$1.5 \pm 0.3 \times 10^{10}$	$4 \pm 1 \times 10^{11}$
k_{trans}^{h}	$3 \pm 1 \times 10^{11}$	10^{12}
k_{rec}^{ex}	$7 \pm 0.3 \times 10^{10}$	$7 \pm 0.3 \times 10^{10}$
k_{rec}^{CT}	$8 \pm 1 \times 10^{9}$	$4 \pm 1\ (0.3 \pm 0.1) \times 10^{9}$
$k_{trans}^{CT,S1}$	$2 \pm 1 \times 10^{9}$	$1 \pm 1 \times 10^{8}$
$k_{trans}^{CT,CS}$	$1 \pm 0.4 \times 10^{10}$	$2 \pm 1\ (0.7 \pm 0.1) \times 10^{9}$
$k_{trans}^{CS,CT}$	$<10^{9}$	$<10^{8}$

[a]The rate constant for exciton recombination (k_{rec}^{ex}) was estimated from the decay of the pristine INDT-S ps-TA signal. The ps-TA spectra of the blends obtained after 450 and 800 nm excitation were fitted with all of the same rate constants, apart from the rate constant describing the initial interconversion of the exciton and CT state, which depends on whether the donor or acceptor was photoexcited (k_{trans}^{e} or k_{trans}^{h}, respectively). k_{rec}^{CT}: rate constant for decay of the CT state to the ground state; $k_{trans}^{CT,CS}$: rate constant for conversion of the CT state into the CS state; $k_{trans}^{CS,CT}$: rate constant for back-transfer from the CS state to the CT state; $k_{trans}^{CT,S1}$: rate constant for back-transfer from the CT state to the exciton state. N.B: when fitting the ps-TA kinetics of the INDT-S:KL blend after 450 nm excitation, the values of the rate constants k_{rec}^{CT} and $k_{trans}^{CT,CS}$ were changed to those shown in brackets.

formation from the exciton state, without changing any other parameter. Interestingly, when assuming perfect collection from the CS state (neglecting any back transfer to the CT state and recombination from the CS state) and using the rates in Table 2, the model predicts a fraction of photogenerated excitons that leads to separated charges that are similar to the IQE values at 800 nm (10% for the INDT-S:PCBM and around 33% for the INDT-S:KL blend) (Figure S12b).

To explain the difference in the V_{oc} of the two devices, we consider the effect of interfacial CT state properties on recombination using a model that we recently developed.[36] From the voltage loss analysis, we have established that the difference in the voltage of the two devices was related to the difference in their nonradiative losses (0.35 V for the PCBM devices and 0.48 V for the KL devices). The properties of the interfacial CT state can be directly related to $\Delta V_{oc,nr}$.[36,37] Because we know that the CT state of INDT-S:PCBM differs from that of INDT-S:KL by having higher energy and f_{OSC} (from the TDDFT calculation and the EL measurement), we implement the differences in these two properties into the model (SI section S13).[36] We find that the 100 meV increase in E_{CT} from INDTS-KL to INDT-S:PCBM first increases V_{oc} by 40 mV, whereas an increase of the CT state f_{OSC} by 2 orders of magnitude increases the V_{oc} by an additional 60 mV, such that their combined effect can explain the change in the V_{oc} between these two devices (Figure 4, Table S6). The simultaneous increase of the CT state energy and its f_{OSC} can be explained by the hybridization of the two states due to the small energy difference between the LUMO levels of the INDT-S:PCBM blend.[38,39] Moreover, the model results show that the total rate of CT state recombination is increased in the PCBM blend relative to the KL case, despite the increased V_{oc}. Although the magnitudes of the recombination rate obtained from the voltage loss models are larger than the experimental ones, the trend in the CT state recombination rate agrees with the results of the fits presented in Table 2. The discrepancy in rates indicates that the model relating recombination to V_{oc} is

DOI: 10.1021/acsenergylett.9b01368
ACS Energy Lett. 2019, 4, 2096−2103

not sufficiently complex to describe experimental systems quantitatively, for example, through neglect of disorder.[40]

Finally, it is important to note that of the two blends considered the one that shows hybridization between the CT and the exciton state has the lower power conversion efficiency. This shows that the reduced voltage losses were insufficient to make up for the losses in the photocurrent upon replacing the KL fullerene with PCBM. However, the hybridization of the CT and exciton states in the INDT-S:PCBM blend has helped to maintain a reasonable efficiency despite the losses in photocurrent. In the absence of hybridization, i.e., with no increase in the oscillator strength relative to INDT-S:KL, as shown in in Table S6, the INDT-S:PCBM blend device V_{oc} would be reduced by 60 mV. This suggest that in some cases the effect of hybridization in increasing the coupling between the CT and the exciton states could result in increases in V_{oc} that overcome any related loss in J_{sc}[38,41,42].

A final issue to address is the possible role of differences in microstructure between the two blends. Differences in excited-state dynamics could, in principle, result from differences in domain size between blends or in the size of pure donor and pure acceptor domains within a blend, with the effect that shorter excited-state lifetimes result for photoexcitation in smaller domains.[28] However, in the studied system, we would expect that PCBM would form larger, more crystalline domains than the less crystallizable KL derivative and that both fullerene derivatives would mix into the polymer at a molecular level. Previous studies of a similar ketolactam fullerene confirm that its tendency to crystallize is weak compared to PCBM.[43] If domain size were dominating excited-state kinetics, then we would see a difference in kinetics upon excitation of the acceptor, whereas in fact we see almost identical kinetics for excitation of the acceptor and differences only upon excitation of the donor. Moreover, the faster lifetime upon donor excitation is observed using the more crystalline fullerene derivative, which we might expect to be less well mixed into the polymer, in contrast to expectation. From this, we conclude that, while variations in microstructure may affect the observed kinetics at some level, they could not explain that large differences in excited-state behavior that we have observed.

In conclusion, in this work, we have studied the effect of the energy offset on the charge carrier dynamics, photocurrent generation, and V_{oc} in polymer:fullerene solar cells. We have found that, despite the insignificant energy offset for electron transfer in the INDT-S:PCBM blend, the charge generation process was significantly more efficient than for the pristine INDT-S devices. From the picosecond dynamics of the photoexcited states, we have established that the low-energy offset results in a lower electron transfer rate from the exciton to the CT state without further affecting the other charge generation processes (compared to the case where the acceptor was photoexcited). On the other hand, the increased V_{oc} for the low-energy offset blend was explained by a coupled effect: an increase in the CT state energy and an increase of the CT state to the ground-state transition's oscillator strength. The increased oscillator strength for the low offset cases is likely to result from mixing of the exciton and CT states and the associated intensity-borrowing mechanism. The study suggests that by careful tuning of the exciton to the CT state offset and consideration of electron and hole transfer contributions high V_{oc} values may be achieved while maintaining useful photocurrents.

■ ASSOCIATED CONTENT

Supporting Information

The Supporting Information is available free of charge on the ACS Publications website at DOI: 10.1021/acsenergylett.9b01368.

Experimental section, ketolactam fullerene synthesis and characterization, KL vs PCBM cyclic voltammetry, absorption spectra, calculation of internal quantum efficiency, EQE of polymer:fullerene blend and pristine polymer devices, voltage loss/electroluminescence, microsecond transient absorption spectroscopy, dependence of the kinetics on the presence of oxygen, picosecond transient absorption spectroscopy spectra, fraction of polymer absorption at key wavelengths, pump−push-photocurrent, TD-DFT calculation of excited states, simulation of transient absorption kinetics using a kinetic model, and nonradiative voltage losses model results (PDF)

■ AUTHOR INFORMATION

Corresponding Author

*E-mail: jenny.nelson@imperial.ac.uk.

ORCID

Mohammed Azzouzi: 0000-0001-5190-9984
Thomas R. Hopper: 0000-0001-5084-1914
Kealan Fallon: 0000-0001-6241-6034
Hugo Bronstein: 0000-0003-0293-8775
Thomas Kirchartz: 0000-0002-6954-8213
Artem A. Bakulin: 0000-0002-3998-2000
Tracey M. Clarke: 0000-0003-4943-0645

Author Contributions

¶M.S.V. and M.A. contributed equally.

Notes

The authors declare no competing financial interest.

■ ACKNOWLEDGMENTS

M.V. and M.A. thank the U.K. Engineering and Physical Sciences Research Council (EPSRC) for postgraduate studentships. J.N. acknowledges funding from the EPSRC (Grant Numbers EP/P005543/1, EP/M025020/1), the EPSRC Supersolar Hub (EP/P02484X/1), and the European Research Council under the European Union's Horizon 2020 research and innovation program (Grant Agreement No 742708). T.M.C. acknowledges support from EPSRC (Grant No. EP/N026411/1). H.B. acknowledges funding from the EU project 679789 − CONTREX. A.A.B. is a Royal Society University Research Fellow. The authors thank Flurin Eisner and Stoichko Dimitrov for their help with the measurements.

■ REFERENCES

(1) Cowan, S. R.; Banerji, N.; Leong, W. L.; Heeger, A. J. Charge Formation, Recombination, and Sweep-out Dynamics in Organic Solar Cells. *Adv. Funct. Mater.* **2012**, *22* (6), 1116−1128.

(2) Brédas, J.-L.; Norton, J. E.; Cornil, J.; Coropceanu, V. Molecular Understanding of Organic Solar Cells: The Challenges. *Acc. Chem. Res.* **2009**, *42* (11), 1691−1699.

(3) Clarke, T. M.; Durrant, J. R. Charge Photogeneration in Organic Solar Cells. *Chem. Rev.* **2010**, *110* (11), 6736−6767.

(4) Dimitrov, S. D.; Bakulin, A. A.; Nielsen, C. B.; Schroeder, B. C.; Du, J.; Bronstein, H.; McCulloch, I.; Friend, R. H.; Durrant, J. R. On the Energetic Dependence of Charge Separation in Low-Band-Gap

DOI: 10.1021/acsenergylett.9b01368
ACS Energy Lett. 2019, 4, 2096−2103

Polymer/Fullerene Blends. *J. Am. Chem. Soc.* **2012**, *134* (44), 18189−18192.
(5) Dimitrov, S. D.; Nielsen, C. B.; Shoaee, S.; Shakya Tuladhar, P.; Du, J.; McCulloch, I.; Durrant, J. R. Efficient Charge Photogeneration by the Dissociation of $PC_{70}BM$ Excitons in Polymer/Fullerene Solar Cells. *J. Phys. Chem. Lett.* **2012**, *3* (1), 140−144.
(6) Bakulin, A. A.; Dimitrov, S. D.; Rao, A.; Chow, P. C. Y.; Nielsen, C. B.; Schroeder, B. C.; McCulloch, I.; Bakker, H. J.; Durrant, J. R.; Friend, R. H. Charge-Transfer State Dynamics Following Hole and Electron Transfer in Organic Photovoltaic Devices. *J. Phys. Chem. Lett.* **2013**, *4* (1), 209−215.
(7) Ohkita, H.; Cook, S.; Astuti, Y.; Duffy, W.; Tierney, S.; Zhang, W.; Heeney, M.; McCulloch, I.; Nelson, J.; Bradley, D. D. C.; et al. Charge Carrier Formation in Polythiophene/Fullerene Blend Films Studied by Transient Absorption Spectroscopy. *J. Am. Chem. Soc.* **2008**, *130* (10), 3030−3042.
(8) Rand, B. P.; Burk, D. P.; Forrest, S. R. Offset Energies at Organic Semiconductor Heterojunctions and Their Influence on the Open-Circuit Voltage of Thin-Film Solar Cells. *Phys. Rev. B: Condens. Matter Mater. Phys.* **2007**, *75* (11), 115327.
(9) Faist, M. A.; Kirchartz, T.; Gong, W.; Ashraf, R. S.; McCulloch, I.; De Mello, J. C.; Ekins-Daukes, N. J.; Bradley, D. D. C.; Nelson, J. Competition between the Charge Transfer State and the Singlet States of Donor or Acceptor Limiting the Efficiency in Polymer: Fullerene Solar Cells. *J. Am. Chem. Soc.* **2012**, *134* (1), 685−692.
(10) Vandewal, K.; Ma, Z.; Bergqvist, J.; Tang, Z.; Wang, E.; Henriksson, P.; Tvingstedt, K.; Andersson, M. R.; Zhang, F.; Inganäs, O. Quantification of Quantum Efficiency and Energy Losses in Low Bandgap Polymer:Fullerene Solar Cells with High Open-Circuit Voltage. *Adv. Funct. Mater.* **2012**, *22* (16), 3480−3490.
(11) Qian, D.; Zheng, Z.; Yao, H.; Tress, W.; Hopper, T. R.; Chen, S.; Li, S.; Liu, J.; Chen, S.; Zhang, J.; et al. Design Rules for Minimizing Voltage Losses in High-Efficiency Organic Solar Cells. *Nat. Mater.* **2018**, *17* (8), 703−709.
(12) Albrecht, S.; Vandewal, K.; Tumbleston, J. R.; Fischer, F. S. U.; Douglas, J. D.; Fréchet, J. M. J.; Ludwigs, S.; Ade, H.; Salleo, A.; Neher, D. On the Efficiency of Charge Transfer State Splitting in Polymer:Fullerene Solar Cells. *Adv. Mater.* **2014**, *26* (16), 2533−2539.
(13) Vandewal, K.; Albrecht, S.; Hoke, E. T.; Graham, K. R.; Widmer, J.; Douglas, J. D.; Schubert, M.; Mateker, W. R.; Bloking, J. T.; Burkhard, G. F.; et al. Efficient Charge Generation by Relaxed Charge-Transfer States at Organic Interfaces. *Nat. Mater.* **2014**, *13* (1), 63−68.
(14) Silva, C. Some like It Hot. *Nat. Mater.* **2013**, *12* (1), 5−6.
(15) Yao, J.; Kirchartz, T.; Vezie, M. S.; Faist, M. A.; Gong, W.; He, Z.; Wu, H.; Troughton, J.; Watson, T.; Bryant, D.; et al. Quantifying Losses in Open-Circuit Voltage in Solution-Processable Solar Cells. *Phys. Rev. Appl.* **2015**, *4* (1), 014020.
(16) Vandewal, K.; Tvingstedt, K.; Gadisa, A.; Inganäs, O.; Manca, J. V. On the Origin of the Open-Circuit Voltage of Polymer−fullerene Solar Cells. *Nat. Mater.* **2009**, *8* (11), 904−909.
(17) Janssen, R. A. J.; Nelson, J. Factors Limiting Device Efficiency in Organic Photovoltaics. *Adv. Mater.* **2013**, *25* (13), 1847−1858.
(18) Azzouzi, M.; Kirchartz, T.; Nelson, J. Factors Controlling Open-Circuit Voltage Losses in Organic Solar Cells. *Trends Chem.* **2019**, *1* (1), 49−62.
(19) Green, M. A.; Ho-Baillie, A. W. Y. Pushing to the Limit: Radiative Efficiencies of Recent Mainstream and Emerging Solar Cells. *ACS Energy Lett.* **2019**, *4* (7), 1639−1644.
(20) Baran, D.; Ashraf, R. S.; Hanifi, D. A.; Abdelsamie, M.; Gasparini, N.; Röhr, J. A.; Holliday, S.; Wadsworth, A.; Lockett, S.; Neophytou, M.; et al. Reducing the Efficiency−stability−cost Gap of Organic Photovoltaics with Highly Efficient and Stable Small Molecule Acceptor Ternary Solar Cells. *Nat. Mater.* **2017**, *16* (3), 363−369.
(21) Ziffer, M. E.; Jo, S. B.; Zhong, H.; Ye, L.; Liu, H.; Lin, F.; Zhang, J.; Li, X.; Ade, H. W.; K-Y Jen, A.; et al. Long-Lived, Non-Geminate, Radiative Recombination of Photogenerated Charges in a Polymer/Small-Molecule Acceptor Photovoltaic Blend. *J. Am. Chem. Soc.* **2018**, *140* (31), 9996−10008.
(22) Sworakowski, J.; Lipiński, J.; Janus, K. On the Reliability of Determination of Energies of HOMO and LUMO Levels in Organic Semiconductors from Electrochemical Measurements. A Simple Picture Based on the Electrostatic Model. *Org. Electron.* **2016**, *33*, 300−310.
(23) Fallon, K. J.; Wijeyasinghe, N.; Manley, E. F.; Dimitrov, S. D.; Yousaf, S. A.; Ashraf, R. S.; Duffy, W.; Guilbert, A. A. Y.; Freeman, D. M. E.; Al-Hashimi, M.; et al. Indolo-Naphthyridine-6,13-Dione Thiophene Building Block for Conjugated Polymer Electronics: Molecular Origin of Ultrahigh n-Type Mobility. *Chem. Mater.* **2016**, *28* (22), 8366−8378.
(24) Sylvester-Hvid, K. O.; Ziegler, T.; Riede, M. K.; Keegan, N.; Niggemann, M.; Gombert, A. Analyzing Poly(3-Hexyl-Thiophene):1-(3-Methoxy-Carbonyl)Propyl-1-Phenyl-(6,6)C61 Bulk-Heterojunction Solar Cells by UV-Visible Spectroscopy and Optical Simulations. *J. Appl. Phys.* **2007**, *102* (5), 054502.
(25) Burkhard, G. F.; Hoke, E. T.; McGehee, M. D. Accounting for Interference, Scattering, and Electrode Absorption to Make Accurate Internal Quantum Efficiency Measurements in Organic and Other Thin Solar Cells. *Adv. Mater.* **2010**, *22* (30), 3293−3297.
(26) Chow, P. C. Y.; Albert-Seifried, S.; Gélinas, S.; Friend, R. H. Nanosecond Intersystem Crossing Times in Fullerene Acceptors: Implications for Organic Photovoltaic Diodes. *Adv. Mater.* **2014**, *26*, 4851−4854.
(27) Yamamoto, S.; Guo, J.; Ohkita, H.; Ito, S. Formation of Methanofullerene Cation in Bulk Heterojunction Polymer Solar Cells Studied by Transient Absorption Spectroscopy. *Adv. Funct. Mater.* **2008**, *18* (17), 2555−2562.
(28) Dimitrov, S. D.; Azzouzi, M.; Wu, J.; Yao, J.; Dong, Y.; Tuladhar, P. S.; Schroeder, B. C.; Bittner, E. R.; McCulloch, I.; Nelson, J.; et al. Spectroscopic Investigation of the Effect of Microstructure and Energetic Offset on the Nature of Interfacial Charge Transfer States in Polymer: Fullerene Blends. *J. Am. Chem. Soc.* **2019**, *141* (11), 4634−4643.
(29) Bakulin, A. A.; Rao, A.; Pavelyev, V. G.; Van Loosdrecht, P. H. M.; Pshenichnikov, M. S.; Niedzialek, D.; Cornil, J.; Beljonne, D.; Friend, R. H. The Role of Driving Energy and Delocalized States for Charge Separation in Organic Semiconductors. *Science* **2012**, *335* (6074), 1340−1344.
(30) Weu, A.; Hopper, T. R.; Lami, V.; Kreß, J. A.; Bakulin, A. A.; Vaynzof, Y. Field-Assisted Exciton Dissociation in Highly Efficient PffBT4T-2OD:Fullerene Organic Solar Cells. *Chem. Mater.* **2018**, *30* (8), 2660−2667.
(31) Few, S.; Frost, J. M.; Kirkpatrick, J.; Nelson, J. Influence of Chemical Structure on the Charge Transfer State Spectrum of a Polymer:Fullerene Complex. *J. Phys. Chem. C* **2014**, *118* (16), 8253−8261.
(32) Bittner, E. R.; Silva, C. Noise-Induced Quantum Coherence Drives Photo-Carrier Generation Dynamics at Polymeric Semiconductor Heterojunctions. *Nat. Commun.* **2014**, *5*, 3119.
(33) Raos, G.; Casalegno, M.; Idé, J. An Effective Two-Orbital Quantum Chemical Model for Organic Photovoltaic Materials. *J. Chem. Theory Comput.* **2014**, *10* (1), 364−372.
(34) Bixon, M.; Jortner, J.; Cortes, J.; Heitele, H.; Michel-Beyerle, M. E. Energy Gap Law for Nonradiative and Radiative Charge Transfer in Isolated and in Solvated Supermolecules. *J. Phys. Chem.* **1994**, *98* (30), 7289−7299.
(35) Braun, C. L. Electric Field Assisted Dissociation of Charge Transfer States as a Mechanism of Photocarrier Production. *J. Chem. Phys.* **1984**, *80* (9), 4157−4161.
(36) Azzouzi, M.; Yan, J.; Kirchartz, T.; Liu, K.; Wang, J.; Wu, H.; Nelson, J. Nonradiative Energy Losses in Bulk-Heterojunction Organic Photovoltaics. *Phys. Rev. X* **2018**, *8* (3), 031055.
(37) Benduhn, J.; Tvingstedt, K.; Piersimoni, F.; Ullbrich, S.; Fan, Y.; Tropiano, M.; McGarry, K. A.; Zeika, O.; Riede, M. K.; Douglas, C. J.; et al. Intrinsic Non-Radiative Voltage Losses in Fullerene-Based Organic Solar Cells. *Nat. Energy* **2017**, *2* (6), 17053.

DOI: 10.1021/acsenergylett.9b01368
ACS Energy Lett. 2019, 4, 2096−2103

(38) Eisner, F. D.; Azzouzi, M.; Fei, Z.; Hou, X.; Anthopoulos, T. D.; Dennis, T. J. S.; Heeney, M.; Nelson, J. Hybridization of Local Exciton and Charge-Transfer States Reduces Nonradiative Voltage Losses in Organic Solar Cells. *J. Am. Chem. Soc.* **2019**, *141* (15), 6362−6374.
(39) Chen, X.-K.; Coropceanu, V.; Brédas, J.-L. Assessing the Nature of the Charge-Transfer Electronic States in Organic Solar Cells. *Nat. Commun.* **2018**, *9* (1), 5295.
(40) D'Avino, G.; Muccioli, L.; Olivier, Y.; Beljonne, D. Charge Separation and Recombination at Polymer−Fullerene Heterojunctions: Delocalization and Hybridization Effects. *J. Phys. Chem. Lett.* **2016**, *7*, 536−540.
(41) Menke, S. M. M.; Cheminal, A.; Conaghan, P.; Ran, N. A. A.; Greehnam, N. C. C.; Bazan, G. C. C.; Nguyen, T.-Q.; Rao, A.; Friend, R. H. H. Order Enables Efficient Electron-Hole Separation at an Organic Heterojunction with a Small Energy Loss. *Nat. Commun.* **2018**, *9* (1), 277.
(42) Han, G.; Yi, Y. Local Excitation/Charge-Transfer Hybridization Simultaneously Promotes Charge Generation and Reduces Nonradiative Voltage Loss in Nonfullerene Organic Solar Cells. *J. Phys. Chem. Lett.* **2019**, *10* (11), 2911−2918.
(43) Ball, J. M.; Bouwer, R. K. M.; Kooistra, F. B.; Frost, J. M.; Qi, Y.; Domingo, E. B.; Smith, J.; De Leeuw, D. M.; Hummelen, J. C.; Nelson, J.; et al. Soluble Fullerene Derivatives: The Effect of Electronic Structure on Transistor Performance and Air Stability. *J. Appl. Phys.* **2011**, *110*, 014506.

DOI: 10.1021/acsenergylett.9b01368
ACS Energy Lett. 2019, 4, 2096−2103